AIAA JOURNAL
Vol. 32, No. 7, July 1994

Aeroelastic Stability of Hingeless Rotor Blade in Hover Using Large Deflection Theory

Maeng Hyo Cho* and In Lee†
Korea Advanced Institute of Science and Technology, Taejon 305-701, Republic of Korea

The coupled flap-lag-torsion aeroelastic stability of a hingeless rotor blade in hover is investigated using finite elements based on large deflection beam theory. The finite element equations of motion for beams undergoing arbitrary large displacements and rotations, but small strains, are obtained from Hamilton's principle. The stability boundary is calculated assuming blade motions to be small perturbations about the nonlinear steady equilibrium deflections, which are obtained through an iterative Newton-Raphson method. The *p-k* modal flutter analysis based on coupled rotating natural modes is used. Various unsteady two-dimensional strip theories are used to evaluate the aerodynamic loads. The sensitivity of the stability boundary to these aerodynamic assumptions is examined. Numerical results of the steady deflections and stability boundaries are presented for some representative blade configurations and also compared with those given in previous moderate deflection type theories.

Nomenclature

a_0 = two-dimensional lift curve slope
$C(k)$ = Theodorsen's lift deficiency function
$C'(k, m, h)$ = Loewy's modified lift deficiency function
c = blade chord length
c_{d0} = profile drag coefficient
$\boldsymbol{e}_1, \boldsymbol{e}_2, \boldsymbol{e}_3$ = triad attached to a reference line of undeformed blade
$\boldsymbol{e}_1^*, \boldsymbol{e}_2^*, \boldsymbol{e}_3^*$ = triad attached to a reference line of deformed blade
$\boldsymbol{g}_i, \boldsymbol{G}_i$ = base vectors of an arbitrary point of the undeformed and deformed blades, respectively ($i = 1, 2, 3$)
h = wake spacing or unsteady plunging motion of blade cross section
I_p = polar moment of inertia of blade cross section, Ak_A^2
$\boldsymbol{i}_1, \boldsymbol{i}_2, \boldsymbol{i}_3$ = triad fixed in a reference frame that rotates with respect to the inertia frame
k = local reduced frequency, $\omega c/2\Omega r$
k_A = polar radius of gyration of blade cross section
k_m = mass radius of gyration of blade cross section, $\sqrt{k_{m_1}^2 + k_{m_2}^2}$
k_{m_1}, k_{m_2} = principal mass radii of gyration of blade cross section
m = frequency ratio, ω/Ω
m_0 = blade reference mass per unit length
N_b = number of blades
p = Laplace operator for the *p-k* method
R = blade radius
r = blade radial coordinate
U_R, U_T, U_P = radial, tangential, and perpendicular components of resultant velocity U in deformed blade coordinate system
u_1, u_2, u_3 = components of displacement vector $\boldsymbol{u}$ in the $\boldsymbol{i}_1, \boldsymbol{i}_2, \boldsymbol{i}_3$ directions, respectively
v_{id} = induced inflow velocity
x_A = aerodynamic center offset from elastic axis and positive for aerodynamic center ahead of elastic axis
x_1, x_2, x_3 = blade curvilinear coordinates
$\alpha_1, \alpha_2, \alpha_3$ = orientation angles between $\boldsymbol{i}_i$ and $\boldsymbol{e}_i^*$ triads in the order ψ (lead-lag angle), β (flap angle), θ (pitch angle)
β_{pc} = blade precone angle
γ = Lock number, $3a_0\rho_a cR/m_0$
ε = unsteady pitching motion of blade cross section
θ_p = blade collective pitch angle
$\lambda(x_2, x_3)$ = section warping function
ρ, ρ_a = mass and air densities, respectively
σ = blade solidity, $N_b c/\pi R$
φ = amplitude of torsional warping
Ω = rotor blade angular velocity
ω = system frequency
$\omega_F, \omega_L, \omega_T$ = nondimensional fundamental coupled rotating flap, lead-lag, and torsion frequencies, respectively

Received April 13, 1993; revision received Nov. 30, 1993; accepted for publication Feb. 7, 1994.

*Graduate Research Assistant, Department of Aerospace Engineering, 373-1 Kusong-dong, Yusong-gu.
†Associate Professor, Department of Aerospace Engineering, 373-1 Kusong-dong, Yusong-gu. Member AIAA.

Introduction

THE aeroelastic stability of a hingeless rotor blade is inherently a nonlinear phenomenon that involves structural, inertial, and aerodynamic loads. The research carried out during the last 20 years has established that the only reliable analyses involve the treatment of the complete coupled flap-lag-torsion problem, and geometrical nonlinearities due to blade deflections play an important role in the aeroelastic stability of the hingeless rotor blade.[1,2]

Most of the structural dynamic models for rotor blades are moderate deflection type beam theories[3,4] that are based on ordering schemes and are valid for moderate deflections. These models have frequently been applied to the aeroelastic stability and response analyses for isotropic[5–8] and composite[9] hingeless rotor blades. However, a general purpose analysis demands the large deflection model without any artificial restrictions on displacements and rotations due to the deformation and the degree of nonlinearity.[10] The ordering scheme, although it can be a valuable tool in special purpose research, is not desirable in a general purpose approach. To overcome these limitations of previous models, structural models that are valid for large deflections and are not based on ordering schemes have been developed during the last few years.[10–15] The only restriction on the deformation in these theories is that the strain is small compared with unity. There are no small-angle approximations made, and all kinematic nonlinear effects are included in the formulation. Recently, nonlinear plate[16] and shell[17] theories based on these approaches were also developed.

A previous nonlinear aeroelastic analysis based on such general formulation can be found in Ref. 18, where numerical results of the nonlinear steady deformation for isotropic rotor blades were obtained. Later, a general rotorcraft aeromechanical stability program[19] was developed, using the aeroelastic beam model based on Ref. 18, and numerical results were presented for the coupled rotor/body problem. Recently, the stability analysis[20] of composite rotor blades based on an exact nonlinear beam theory[15] has also been performed.

In this paper, the aeroelastic stability for an isotropic hingeless rotor blade undergoing arbitrary large deflections and rotations in

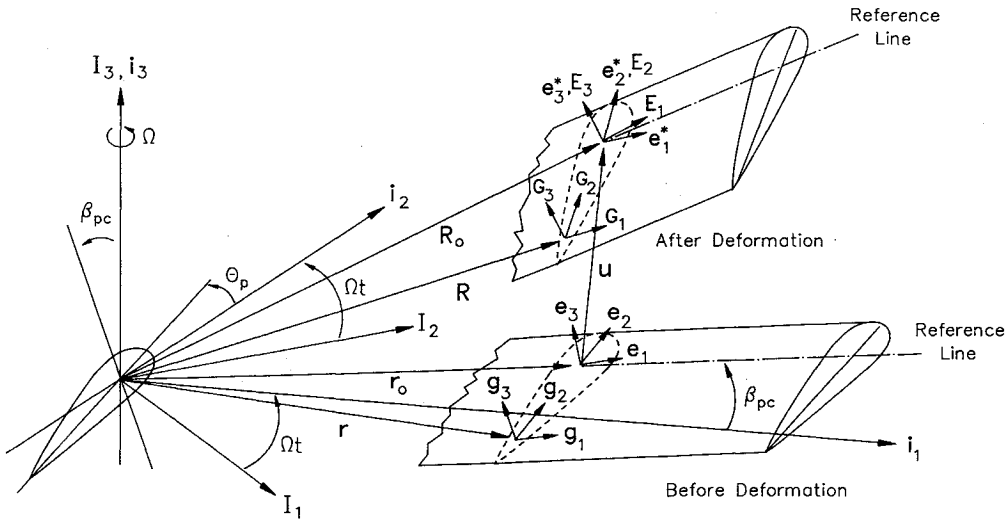

Fig. 1 Geometry and coordinate systems of a rotor blade before and after deformation.

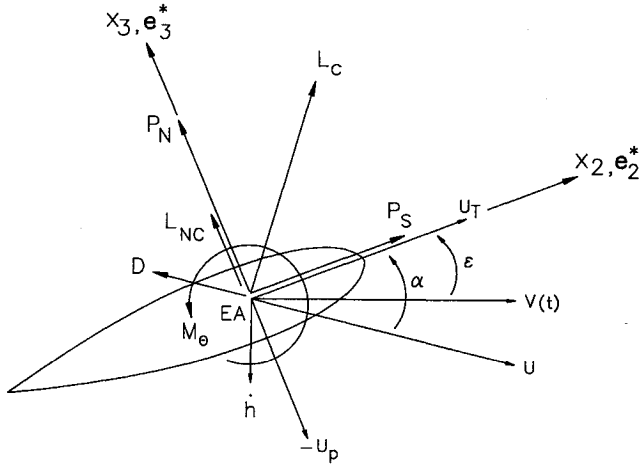

Fig. 2 Rotor blade airfoil section in general unsteady motion.

the hovering flight condition has been investigated. The structural model used in the present analysis is based on Bauchau and Hong's beam model,[14] which utilizes orientation angles to represent large rotations. Transverse shearing deformations and torsional warping effects are included in the formulation. The finite element equations of motion derived from Hamilton's principle are solved for the steady blade deformation using the Newton-Raphson method. After performing the coupled rotating free vibration analysis of the blade about the equilibrium position, the *p-k* method based on these natural modes is used to solve the linearized stability equations. The unsteady two-dimensional aerodynamic models considered in the present analysis are the quasisteady theory, Greenberg's extension[21] of Theodorsen's theory, and Loewy's theory[22] including effect of the spiral returning wake beneath a hovering rotor. The sensitivity of the stability boundary to these aerodynamic assumptions is examined. The steady deflections and stability boundaries for typical representative rotor blade configurations are compared with those by some of the previous moderate deflection type theories. The influence of the preconing and the offset between the aerodynamic center and the elastic axis on the linearized aeroelastic stability is investigated for the cantilevered rotor blade with uniform section properties.

Analysis

Blade Structural Model

Consider the rotor blade rotating with constant angular velocity Ω depicted in Fig. 1. Here the triad $\boldsymbol{I}_1, \boldsymbol{I}_2$, and $\boldsymbol{I}_3$ is fixed in an inertia frame; the triad $\boldsymbol{i}_1, \boldsymbol{i}_2$, and $\boldsymbol{i}_3$ is fixed in a reference frame which rotates with respect to the inertia frame at a constant angular velocity $\Omega \boldsymbol{I}_3$; and the triad $\boldsymbol{e}_1, \boldsymbol{e}_2$, and $\boldsymbol{e}_3$ is attached to a reference line along the axis of the undeformed blade. The curvilinear coordinates along this triad are x_1, x_2, and x_3, respectively. The terms $\boldsymbol{e}_i$ and $\boldsymbol{E}_i$ $(i = 1, 2, 3)$ are the base vectors at the positions $\boldsymbol{r}_0(x_1, 0, 0)$ and $\boldsymbol{R}_0(x_1, 0, 0)$ of the reference line, and $\boldsymbol{g}_i$ and $\boldsymbol{G}_i$ are the base vectors at the positions $\boldsymbol{r}$ and $\boldsymbol{R}$ of an arbitrary point of the cross section in the undeformed and deformed blade configurations, respectively. After deformation, $\boldsymbol{E}_1$ is no longer unit or orthogonal to $\boldsymbol{E}_2$ or $\boldsymbol{E}_3$, since axial and shearing strains are allowed, and thus new triad $\boldsymbol{e}_i^*$ is defined as follows: $\boldsymbol{e}_2^* = \boldsymbol{E}_2, \boldsymbol{e}_3^* = \boldsymbol{E}_3$, and $\boldsymbol{e}_1^* = \boldsymbol{e}_2^* \times \boldsymbol{e}_3^*$. Assuming that the initial curvatures are small and the axial and shearing strains are much smaller than unity in the Green-Lagrangian strain components (for more details see Ref. 14), the axial strain component ε_{11} and the transverse shearing strain components γ_{12} and γ_{13} are expressed as follows:

$$\begin{aligned}\varepsilon_{11} &= \bar{e}_{11} - x_2\kappa_3 + x_3\kappa_2 + \lambda\varphi' + k_1(x_3\lambda_{,2} - x_2\lambda_{,3})\varphi \\ &\quad + (1/2)(2\bar{e}_{12} - x_3\kappa_1)^2 + (1/2)(2\bar{e}_{13} + x_2\kappa_1)^2 \\ \gamma_{12} &= 2\bar{e}_{12} - x_3\kappa_1 + \lambda_{,2}\varphi \\ \gamma_{13} &= 2\bar{e}_{13} + x_2\kappa_1 + \lambda_{,3}\varphi\end{aligned} \tag{1}$$

where $\lambda(x_2, x_3)$ is the Saint Venant warping function and $\varphi(x_1)$ the warping amplitude; $(.)'$ means the derivative with respect to x_1, $(.)_{,i}$ derivatives with respect to x_i, $i = 2, 3$. The force strains $(\bar{e}_{11}, 2\bar{e}_{12}, 2\bar{e}_{13})$ and moment strains $(\kappa_1, \kappa_2, \kappa_3)$ components are given by

$$\begin{Bmatrix}\bar{e}_{11}\\ 2\bar{e}_{12}\\ 2\bar{e}_{13}\end{Bmatrix} = \boldsymbol{T}(x_1)\begin{Bmatrix}u_1' + t_{11}\\ u_2' + t_{12}\\ u_3' + t_{13}\end{Bmatrix} - \begin{Bmatrix}1\\0\\0\end{Bmatrix} \tag{2}$$

$$\begin{Bmatrix}\kappa_1\\ \kappa_2\\ \kappa_3\end{Bmatrix} = \begin{bmatrix}s_2 & 0 & 1\\ c_2s_3 & -c_3 & 0\\ c_2s_3 & s_3 & 0\end{bmatrix}\begin{Bmatrix}\alpha_1\\ \alpha_2\\ \alpha_3\end{Bmatrix} - \begin{Bmatrix}k_1\\ k_2\\ k_3\end{Bmatrix} \tag{3}$$

where u_i are the components of the displacement vector $\boldsymbol{u}$ in the basic reference triad $\boldsymbol{i}_i$. The transformation matrix $\boldsymbol{T}$ from the triad $\boldsymbol{i}_i$ to the triad $\boldsymbol{e}_i^*$ is defined as $\boldsymbol{e}_i^* = \boldsymbol{T}_{ij}\boldsymbol{i}_j$; $c_i = \cos\alpha_i$ and $s_i = \sin\alpha_i$; and t_{11}, t_{12}, t_{13} are the components of the transformation matrix from $\boldsymbol{i}_i$ to $\boldsymbol{e}_i$. The pretwist is k_1, and the initial curvatures of the blade are k_2 and k_3.

The equations of motion for a hingeless isotropic rotor blade are obtained using Hamilton's principle:

$$\int_{t_1}^{t_2} (\delta U - \delta T - \delta W)\, dt = 0 \tag{4}$$

where

$$\delta U = \int_0^L \left(\int_A \begin{Bmatrix} \delta\varepsilon_{11} \\ \delta\gamma_{12} \\ \delta\gamma_{13} \end{Bmatrix}^T \begin{bmatrix} E & 0 & 0 \\ 0 & Gk_s & 0 \\ 0 & 0 & Gk_s \end{bmatrix} \begin{Bmatrix} \varepsilon_{11} \\ \gamma_{12} \\ \gamma_{13} \end{Bmatrix} dA \right) dx_1$$

$$\delta T = \int_0^L \left(\int_A \rho \delta \boldsymbol{V} \cdot \boldsymbol{V}\, dA \right) dx_1$$

$$\delta W = \int_0^L \left(\int_A \delta \boldsymbol{R} \cdot \boldsymbol{f}\, dA \right) dx_1$$

where δU, δT, and δW are the variation of strain energy, the variation of kinetic energy, and the virtual work of applied forces, respectively; L is the blade length, E is Young's modulus, G is the shear modulus, k_s the transverse shear correction factor, ρ the mass density of the blade, $\boldsymbol{V}$ the velocity with respect to the inertia frame ($\boldsymbol{V} = \dot{\boldsymbol{R}} + \Omega \boldsymbol{I}_3 \times \boldsymbol{R}$), and $\boldsymbol{f}$ the external aerodynamic force.

Unsteady Aerodynamic Model

The aerodynamic lift and pitching moment acting on the blade in hover are based on Greenberg's extension[21] of Theodorsen's theory for a two-dimensional airfoil undergoing unsteady motion in an incompressible flow. Consider the rotor blade airfoil section undergoing general unsteady pitching $\varepsilon(t)$ and plunging $h(t)$ motions for freestream velocity $V(t)$ depicted in Fig. 2. Assuming that the pitching angle ε and the angle of attack α are small, the expressions for the force components P_S and P_N acting on the deformed blade section and pitching moment component M_θ may be written as[5,23]

$$\begin{aligned} P_S &= -a_0 \rho_a b C(k) \left[-U_P^2 + b(1/2 - a) U_P \dot{\varepsilon} \right] - \rho_a b c_{d_0} U_T^2 \\ P_N &= a_0 \rho_a b C(k) \left[-U_P U_T + b(1/2 - a) U_T \dot{\varepsilon} \right] \\ &\quad + (1/2) a_0 \rho_a b^2 (-\dot{U}_P - b a \ddot{\varepsilon}) - \rho_a b c_{d_0} U_P U_T \\ M_\theta &= a_0 \rho_a b^2 (1/2 + a) C(k) \left[-U_P U_T + b(1/2 - a) U_T \dot{\varepsilon} \right] \\ &\quad + (1/2) a_0 \rho_a b^2 \left[-b a \dot{U}_P - (1/2) U_T b \dot{\varepsilon} - b^2 (1/8 + a^2) \ddot{\varepsilon} \right] \end{aligned} \tag{5}$$

where $a = x_A - 1/2$ (x_A: positive for the aerodynamic center ahead of the elastic axis), b is the semichord, and $C(k)$ is replaced by a more complicated function $C'(k, m, h)$ in Loewy's theory. The velocity $\boldsymbol{U}$ is the resultant of the induced inflow velocity v_{id} ($=\Omega R \lambda_i$) and the blade elastic velocity $\boldsymbol{V}$ at a point on the elastic axis and resolves into three components U_R (radial), U_T (tangential), and U_P (perpendicular) with respect to the deformed blade coordinate system. The expressions for the components of resultant velocity $\boldsymbol{U}$ are given by

$$\begin{Bmatrix} U_R \\ U_T \\ U_P \end{Bmatrix} = \boldsymbol{T} \begin{Bmatrix} \dot{u}_1 - \Omega R_{0_2} \\ \dot{u}_2 + \Omega R_{0_1} \\ \dot{u}_3 + \Omega R \lambda_i \end{Bmatrix} \tag{6}$$

where λ_i is the uniform and steady inflow ratio, and the radial component U_R is negligible in hover. Including the contribution of the angular velocity Ω of a rotating blade, the component $\dot{\varepsilon}$ of angular velocity along the deformed reference line ($\boldsymbol{e}_1^*$ direction) is expressed as $\dot{\varepsilon} = \dot{\theta} + (\Omega + \dot{\psi}) \sin\beta$.

Finite Element Equations and Solution Procedure

The finite element equations of motion can be formulated using the Lagrangian elements with C^0 = continuity as the shear deformation of the blade is allowed. Applying the standard finite element technique to Hamilton's principle (4), we obtain the nonlinear finite element equations of motion in the matrix form:

$$[\boldsymbol{M}(\boldsymbol{q})]\ddot{\boldsymbol{q}} + [\boldsymbol{G}(\boldsymbol{q})]\dot{\boldsymbol{q}} + \boldsymbol{P}(\boldsymbol{q}) - \boldsymbol{P}_C(\boldsymbol{q}) = [\boldsymbol{A}(k, \boldsymbol{q})]\boldsymbol{q} + \boldsymbol{P}_A(\boldsymbol{q}) \tag{7}$$

where $[\boldsymbol{M}]$, $[\boldsymbol{G}]$, and $[\boldsymbol{A}]$ are the mass, gyroscopic damping, and unsteady aerodynamic matrices in finite elements, respectively. The term $\boldsymbol{P}$ is the internal elastic force vector, $\boldsymbol{P}_C$ is the centrifugal load vector, $\boldsymbol{P}_A$ is the steady aerodynamic load vector, and $\boldsymbol{q} = \{\boldsymbol{q}_{u_i}, \boldsymbol{q}_{\alpha_i}, \boldsymbol{q}_\varphi\}^T$ is the generalized nodal displacement vector. Here, the unsteady aerodynamic matrix $[\boldsymbol{A}]$ includes the real apparent mass matrix and the complex aerodynamic damping matrix associated with $C(k)$.

To solve the governing equations of motion (7), the steady-state deformation due to steady aerodynamic loads and centrifugal forces is determined first. By dropping all time-dependent terms, the steady equilibrium equations are obtained: $\boldsymbol{P}(\boldsymbol{q}_0) - \boldsymbol{P}_C(\boldsymbol{q}_0) = \boldsymbol{P}_A(\boldsymbol{q}_0)$. The nonlinear steady deformation $\boldsymbol{q}_0$ is calculated through the iterative Newton-Raphson method. Assuming that the flutter motion is a small perturbation $\tilde{\boldsymbol{q}}(t)$ about the equilibrium position $\boldsymbol{q}_0$, that is, $\boldsymbol{q}(t) = \boldsymbol{q}_0 + \tilde{\boldsymbol{q}}(t)$, then the linearization of Eq. (7) leads to the following equations:

$$[\boldsymbol{M}(\boldsymbol{q}_0)]\ddot{\tilde{\boldsymbol{q}}} + [\boldsymbol{G}(\boldsymbol{q}_0)]\dot{\tilde{\boldsymbol{q}}} + [\boldsymbol{K}(\boldsymbol{q}_0)]\tilde{\boldsymbol{q}} - [\boldsymbol{A}(k, \boldsymbol{q}_0)]\tilde{\boldsymbol{q}} = 0 \tag{8}$$

where $\boldsymbol{K}(\boldsymbol{q}_0)$ is the unsymmetric tangent stiffness matrix including internal elastic, centrifugal, and steady aerodynamic terms. It is well known that the modal representation is convenient for reducing a matrix size and for identifying the flutter mode. The preceding linearized flutter equations are transformed to the modal space by the expression of $\tilde{\boldsymbol{q}} = [\boldsymbol{E}]y$, where $\boldsymbol{E}$ is the modal matrix of the first m coupled rotating modes, and $\boldsymbol{y}$ is the vector of m generalized coordinates in the modal space. The transformed modal equations are solved through the p-k modal flutter analysis discussed in Refs. 24 and 25.

Numerical Results and Discussion

Information for the Computation of the Stability Boundary

In computing the numerical results, a number of simplifying assumptions are made in this paper. Mass and stiffness properties along the span of a blade are assumed to be constant. The correction of the transverse shear deformation is not considered, i.e., $k_s = 1$. Assuming that the cross section is doubly symmetric, the present beam model is formulated by I_p (polar moment of inertia) for the torsional twist angle and D (section warping integral defined in Ref. 26) for the warping amplitude. Thus, to consider the warping deformation, a small value of D corresponding to 0.1% of I_p is used, but the other section integrals including the warping are taken to be zero as in Refs. 5 and 8.

In the nonlinear steady analysis, the unknown functions are seven, i.e., three displacements, three orientation angles, and the amplitude of the torsional warping. However, the linearized stability is analyzed using the reduced tangent stiffness matrix obtained through the Guyan reduction procedure, since the warping degrees of freedom are not included in kinetic energy and virtual work of aerodynamic loadings. For the given polar area radius of gyration k_A, mass radius of gyration k_m, and principal mass radii of gyration k_{m_1} (flapwise) and k_{m_2} (chordwise), the section stiffnesses are chosen iteratively until the nondimensional fundamental coupled rotating frequencies in the flap (ω_F), lead-lag (ω_L), and torsion (ω_T) directions become the given numerical values.

The induced velocity v_{id} is taken to be steady and uniform along the blade radius and is set equal to the value of inflow given by the

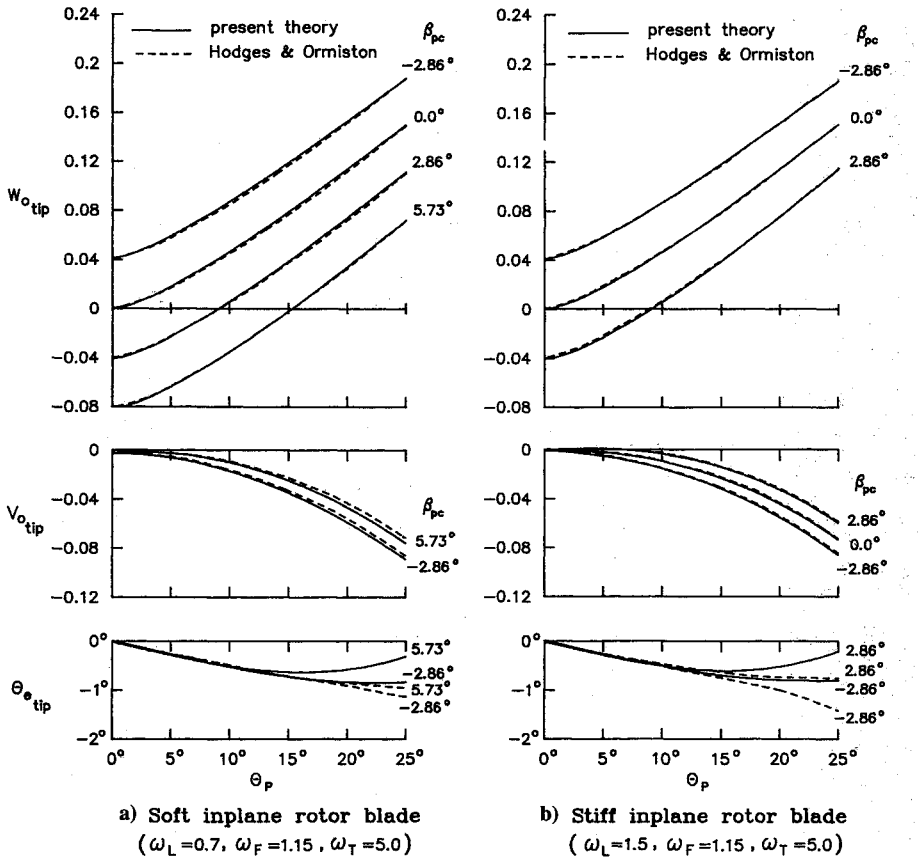

Fig. 3 Comparison of steady tip deflections by the moderate deflection model and the present large deflection model.

combined momentum and blade element theory at radial station $r = 0.75R$. Thus the inflow ratio is expressed as

$$\lambda_i = \frac{v_{id}}{\Omega R} = \frac{\sigma a_0}{16} sign(\theta_{0.75R}) \left[\sqrt{1 + \frac{24}{\sigma a_0} |\theta_{0.75R}|} - 1 \right] \quad (9)$$

where $\theta_{0.75R} = \theta_p + \theta_e(0.75R)$, and θ_e is the elastic twist angle. The blade collective pitch θ_p is varied throughout the nominal range of thrust including very high thrust conditions ($\theta_p > 15$ deg).

Loewy's lift deficiency function $C'(k, m, h)$ including the effect of the spiral returning wake beneath a hovering rotor is given by[22]

$$C'(k, m, h) = \frac{H_1^{(2)}(k) + 2J_1(k)W}{H_1^{(2)}(k) + iH_0^{(2)}(k) + 2W[J_1(k) + iJ_0(k)]} \quad (10)$$

where $H_n^{(2)}$ and J_n are Hankel and Bessel functions, and W is the wake factor. If $W = 0$, the equation becomes Theodorsen's function $C(k)$. The function C' is taken to be unity for a quasisteady approximation of the unsteady theory. To investigate the sensitivity of the stability boundary to these aerodynamic assumptions, $W = 1/[\exp(kh/b)\exp(i2\pi m/N_b) - 1]$ for the collective interblade modes of the multiblade rotor is used in this study. Also all of the unsteady aerodynamic coefficients used are based on the value k evaluated at $r = 0.8R$.[7]

The chordwise offsets of the center of mass and tension center from the elastic axis are considered to be zero. The following common parameters (configurations and operating condition parameters) are used in the calculations:

$$k_m = 0.025, \quad k_{m_1}/k_{m_2} = 0.0, \quad (k_A/k_m)^2 = 1.5$$

$$\gamma = 5, \quad \sigma = 0.1, \quad N_b = 4, \quad c/R = \pi/40 \quad (11)$$

$$a_0 = 2\pi, \quad c_{d_0} = 0.01$$

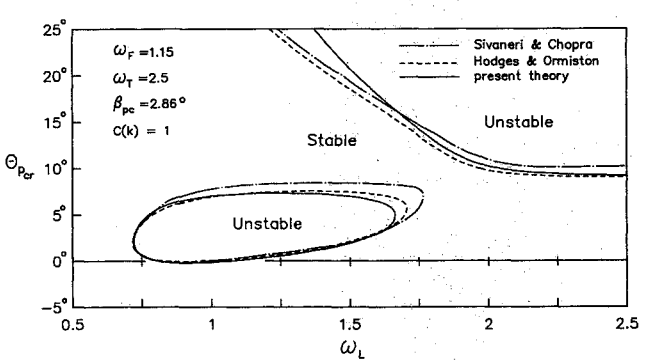

Fig. 4 Comparison of stability boundaries by the moderate deflection models and the present large deflection model.

Finally, the numerical results in this paper are obtained using four noded elements (cubic interpolation functions). Six elements and seven coupled rotating modes with the reasonably good convergence are used in this study.

Results

The fundamental rotating flap frequency ω_F used in this analysis is 1.15, which is representative of typical hingeless blade configurations. The steady tip deflections of typical hingeless soft (ω_L = 0.7) and stiff (ω_L = 1.5) in-plane rotor blades are given in Fig. 3. This figure also shows the results of Hodges and Ormiston[5] obtained by the Galerkin method using the assumed mode shapes and the moderate deflection theory. Two bending nondimensional deflections $v_{0_{tip}}$ (lead-lag) and $w_{0_{tip}}$ (flap) are measured from the e_2 and e_3 axes attached to an undeformed blade, respectively. The agreement between the results of two models for the bending deflections is good, although a slight deviation appears. However, the difference between the two results for the elastic twist angle $\theta_{e_{tip}}$ appears at high thrust levels ($\theta_p > 15$ deg). This may be due to

the assumptions in Ref. 5 that only the second-order nonlinearity is allowed through the ordering scheme in the governing equations, which may not be very accurate at high values of θ_p. No such assumptions are made in the large deflection theory. Figure 4 presents the stability boundaries for the blade configuration with β_{pc} = 2.86 deg (0.05 rad) as the lead-lag frequency ω_L is varied. The results of Sivaneri and Chopra[8] in addition to Hodges and Ormiston are also shown. Sivaneri and Chopra obtained the flutter boundaries by using the moderate deflection type finite elements that include the nonlinear second-order terms. There is a general agreement between the results of two moderate deflection models. However, as seen in Fig. 3, the deviation between the results obtained by moderate deflection models and those by the large deflection model appears at high thrust levels.

The effects of the precone and the various two-dimensional aerodynamic strip theories are illustrated in Fig. 5. The unstable region in this figure corresponds to the bubblelike region shown in Fig. 4 and appears at low values of the collective pitch θ_p. The stability boundaries spread out as the precone increases. When $x_A = 0$, the stability boundary for the typical blade configuration is insensitive to the type of unsteady aerodynamics.

The sensitivity of the stability boundary to the unsteady aerodynamics [$C(k)$ or $C'(k, m, h)$] is explored in Fig. 6. When there exists a destabilizing offset, $x_A = 0.1$ (5% of the chord) between the aerodynamic center and the elastic axis, the type of aerodynamics

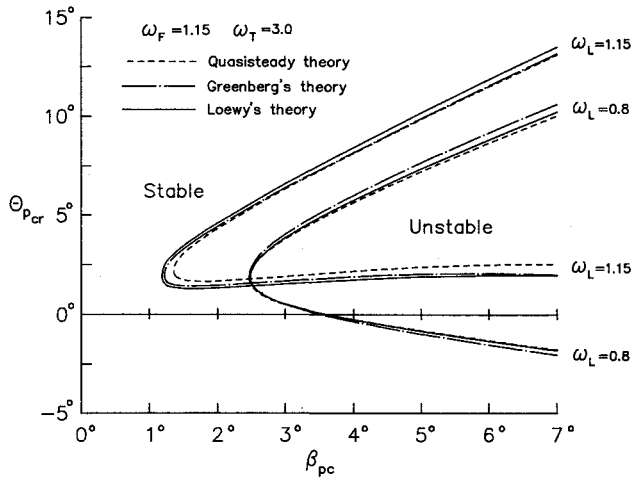

Fig. 5 Effect of precone and various unsteady aerodynamics on the stability boundaries.

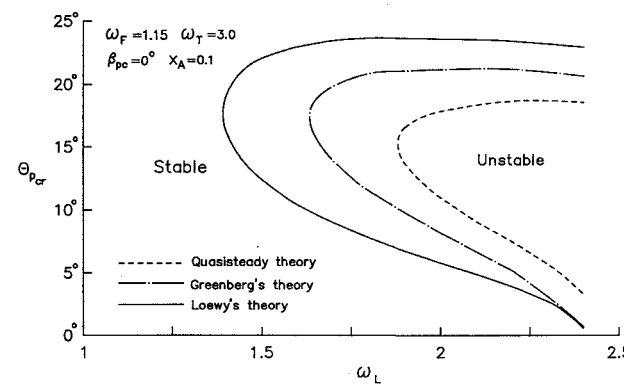

Fig. 6 Effect of offset x_A and various unsteady aerodynamics on the stability boundaries.

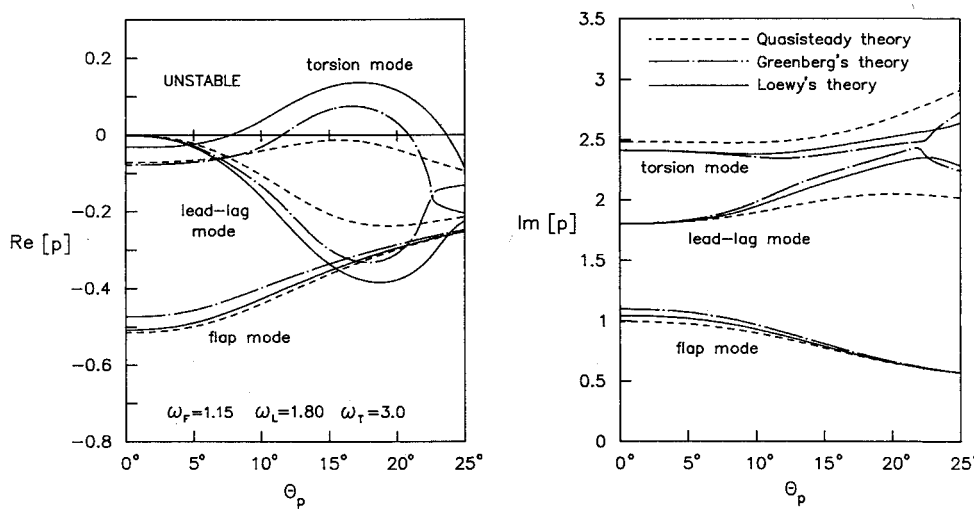

Fig. 7 p-θ_p diagram for a typical blade configuration with β_{pc} = 0 deg and x_A = 0.1.

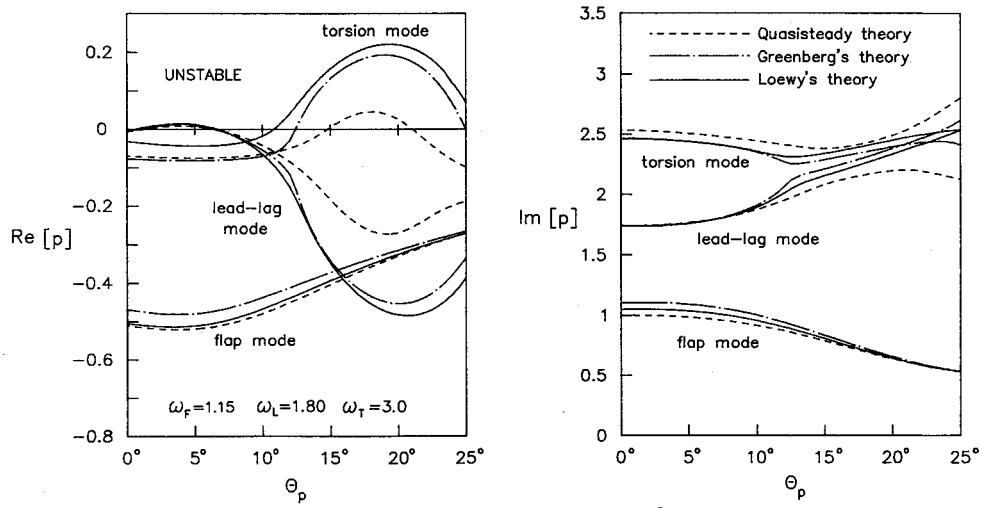

Fig. 8 p-θ_p diagram for a typical blade configuration with β_{pc} = 3 deg and x_A = 0.1.

affects considerably the stability boundary. Especially, it is shown that the effect of Loewy's unsteady aerodynamic theory including the returning wake is noticeable for the stiff-inplane blade configurations. Figure 7 shows the p-θ_p diagram for a typical blade configuration with $\beta_{pc} = 0$ deg and $x_A = 0.1$. The real and imaginary parts of p represent the modal damping and frequency, respectively. When the real part of p becomes positive, the instability occurs. The instability with offset x_A occurs in the torsion mode, whereas the lead-lag mode is usually unstable for the zero offset configuration. Thus it is very interesting to note that the torsional mode instability of the hingeless rotor blade is very sensitive to the type of unsteady aerodynamics.

Finally, the combined effect of the precone and offset x_A is illustrated in Fig. 8. Here, the precone angle β_{pc} is 3 deg and the destabilizing offset x_A is 0.1. The two sets of unstable regions are shown in this figure. One instability associated with the precone appears at low collective pitch and corresponds to the lead-lag mode instability. The other associated with offset x_A appears at high collective pitch and corresponds to the torsion mode instability.

Conclusions

In this paper, the aeroelastic stability of a hingeless rotor blade undergoing arbitrary large deflections and rotations in hover has been investigated. The finite element formulation is obtained using the large deflection type model not based on the ordering scheme. The linearized stability boundary about equilibrium is found from the p-k method after reducing nodal degrees of freedom through a normal mode transformation. The effects of the precone and the offset between the aerodynamic center and the elastic axis on the instability are studied.

The results for steady tip deflections and stability boundaries of typical hingeless rotor blades are compared with those of previous moderate deflection type models. The agreement between those results is good except at very high thrust levels where the structural modeling, which is valid for large deflections, is required. The instability for the rotor blades with the precone occurs along the lead-lag mode branch at low collective pitch settings. For the blade configuration with offset between the aerodynamic center and the elastic axis, the instability occurs in the torsion mode and such a torsional instability is very sensitive to the type of unsteady aerodynamics.

References

[1]Ormiston, R. A., "Investigation of Hingeless Rotor Stability," *Vertica*, Vol. 7, No. 2, 1983, pp. 143–181.

[2]Friedmann, P. P., "Rotary-Wing Aeroelasticity with Application to VTOL Vehicles," *Proceedings of the AIAA/ASME/ASCE/AHS/ACS 31st Structures, Structural Dynamics, and Materials Conference* (Long Beach, CA), AIAA, Washington, DC, 1990, pp. 1624–1670 (AIAA Paper 90-1115).

[3]Hodges, D. H., and Dowell, E. H., "Nonlinear Equations of Motion for Elastic Bending and Torsion of Twisted Non-Uniform Rotor Blades," NASA TN D-7818, Dec. 1974.

[4]Rosen, A., and Friedmann, P. P., "The Nonlinear Behavior of Elastic Slender Straight Beams Undergoing Small Strains and Moderate Rotations," *ASME Journal of Applied Mechanics*, Vol. 46, No. 1, 1979, pp. 161–168.

[5]Hodges, D. H., and Ormiston, R. A., "Stability of Elastic Bending and Torsion of Uniform Cantilever Rotor Blade in Hover with Variable Structural Coupling," NASA TN D-8192, April 1976.

[6]Friedmann, P. P., "Influence of Modeling and Blade Parameters on the Aeroelastic Stability of a Cantilevered Rotor," *AIAA Journal*, Vol. 15, No. 2, 1977, pp. 149–158.

[7]Friedmann, P. P., "Effect of Modified Aerodynamic Strip Theories on Rotor Blade Aeroelastic Stability," *AIAA Journal*, Vol. 15, No. 7, 1977, pp. 932–940.

[8]Sivaneri, N. T., and Chopra, I., "Dynamic Stability of a Rotor Blade Using Finite Element Analysis," *AIAA Journal*, Vol. 20, No. 5, 1982, pp. 716–723.

[9]Hong, C. H., and Chopra, I., "Aeroelastic Stability Analysis of a Composite Rotor Blade," *Journal of the American Helicopter Society*, Vol. 30, No. 2, 1985, pp. 57–67.

[10]Hinnant, H. E., and Hodges, D. H., "Nonlinear Analysis of a Cantilever Beam," *AIAA Journal*, Vol. 26, No. 12, 1988, pp. 1521–1527.

[11]Danielson, D. A., and Hodges, D. A., "A Beam Theory for Large Global Rotation, Moderate Local Rotation, and Small Strain," *ASME Journal of Applied Mechanics*, Vol. 55, March 1988, pp. 179–184.

[12]Atilgan, A. R., and Hodges, D. H., "Unified Nonlinear Analysis for Nonhomogeneous Anisotropic Beams with Closed Cross Sections," *AIAA Journal*, Vol. 29, No. 11, 1991, pp. 1990–1999.

[13]Bauchau, O. A., and Hong, C. H., "Large Displacement Analysis of Naturally Curved and Twisted Composite Beams," *AIAA Journal*, Vol. 25, No. 11, 1987, pp. 1469–1475.

[14]Bauchau, O. A., and Hong, C. H., "Nonlinear Composite Beam Theory," *ASME Journal of Applied Mechanics*, Vol. 55, March 1988, pp. 156–163.

[15]Hodges, D. H., "A Mixed Variational Formulation Based on Exact Intrinsic Equations for Dynamics of Moving Beams," *International Journal of Solids and Structures*, Vol. 26, No. 11, 1990, pp. 1253–1273.

[16]Hodges, D. H., Atilgan, A. R., and Danielson, D. A., "A Geometrically Nonlinear Theory of Elastic Plates," *Proceedings of the AIAA/ASME/ASCE/AHS/ACS 33rd Structures, Structural Dynamics, and Materials Conference* (Dallas, TX), AIAA, Washington, DC, 1992, pp. 878–889 (AIAA Paper 92-2281).

[17]Bauchau, O. A., and Chiang, W., "Dynamic Analysis of Rotor Flexbeams Based on Nonlinear Anisotropic Shell Models," *Journal of the American Helicopter Society*, Vol. 38, Jan. 1993, pp. 55–61.

[18]Hodges, D. H., "Nonlinear Equations for the Dynamics of Pretwisted Beams Undergoing Small Strains and Large Rotations," NASA TP-2470, May 1985.

[19]Hodges, D. H., Hopkins, A. S., Kunz, D. L., and Hinnant, H. E., "Introduction to GRASP—General Rotorcraft Aeromechanical Stability Program—A Modern Approach to Rotorcraft Modeling," *Journal of the American Helicopter Society*, Vol. 32, No. 2, 1987, pp. 78–90.

[20]Fulton, M. V., and Hodges, D. H., "Application of Composite Rotor Blade Stability Analysis to Extension-Twist Coupled Blades," *Proceedings of the AIAA/ASME/ASCE/AHS/ACS 33rd Structures, Structural Dynamics and Materials Conference* (Dallas, TX), AIAA, Washington, DC, 1992, pp. 1989–1995 (AIAA Paper 92-2254).

[21]Greenberg, J. M., "Airfoil in Sinusoidal Motion in a Pulsating Stream," NACA TN-1326, June 1947.

[22]Loewy, R. G., "A Two-Dimensional Approximation to the Unsteady Aerodynamics of Rotary Wings," *Journal of the Aeronautical Sciences*, Vol. 24, No. 2, 1957, pp. 81–92.

[23]Kaza, K. V., and Kvaternik, R. G., "Application of Unsteady Airfoil Theory to Rotary Wings," *AIAA Journal*, Vol. 18, No. 7, 1981, pp. 604–605.

[24]Hassig, H. J., "An Approximate True Damping Solution of the Flutter Equation by Determinant Iteration," *Journal of Aircraft*, Vol. 8, No. 11, 1971, pp. 885–889.

[25]Yamane, T., and Friedmann, P. P., "Aeroelastic Tailoring Analysis for Preliminary Design of Advanced Turbo Propellers with Composite Blades," *Journal of Aircraft*, Vol. 30, No. 1, 1993, pp. 119–126.

[26]Hodges, D. H., "Torsion of Pretwisted Beam Due to Axial Loading," *ASME Journal of Applied Mechanics*, Vol. 47, June 1980, pp. 393–397.